Nuclear Physics A430 (1984) 84–98

E2 CORE POLARIZATION FOR sd-SHELL SINGLE-PARTICLE STATES CALCULATED WITH A SKYRME-TYPE INTERACTION

H. SAGAWA and B.A. BROWN

Cyclotron Laboratory, Michigan State University, East Lansing, MI 48824-1321, USA

Received 6 April 1984
(Revised 14 May 1984)

Abstract: We have studied the core-polarization effect on the 1s0d-shell single-particle electromagnetic quadrupole transitions due to coupling with the quadrupole giant resonances. The self-consistent Hartree–Fock + RPA method is applied for the calculations of the single-particle wave functions and the response functions of the giant resonances. The particle–vibration-coupling model is used to calculate the core-polarization effect in the vicinity of ^{16}O and ^{40}Ca. The effective coupling hamiltonian is determined by the SGII Skyrme-type interaction which is used in the HF + RPA and particle–vibration-coupling calculation. The results are discussed for the proton and neutron effective charges and for the longitudinal and transverse form factor for the $0d_{3/2}^{-1} \rightarrow 1s_{1/2}^{-1}$ proton single-particle transition in ^{39}K. Good agreement with recent longitudinal data for this transition is obtained.

1. Introduction

Electron scattering is a powerful method for studying the density and current distributions in both the ground state and in transitions to the excited nuclear states. The longitudinal form factors are determined by the density distributions. The transverse form factor gives us also information about the current distribution. Shell-model calculations, carried out within a model space in which the nucleons are restricted to occupy a few orbits near the Fermi surface, have been compared with the experimental longitudinal quadrupole (C2) form factors of nuclei over a broad region of the mass table [some recent references are ref. [1]) for the sd shell, ref. [2]) for the fp shell, and ref. [3]) for ^{90}Zr]. However, the comparison for the strong transitions always shows that the theoretical form factors at the first maximum as well as the γ-decay transition probabilities are smaller (typically by about a factor of four) than experiment. Empirically this has been taken care of by introducing "effective charges" for the protons and neutrons. Much theoretical work has been done in order to understand the microscopic origin of these effective charges. Their magnitudes can be qualitatively understood by the coherent mixing of the 1p1h "giant quadrupole" excitation into the low-lying states. This effect can be regarded as a polarization of the core protons by the valence protons and neutrons [4]) and is often referred to as the "core-polarization" effect. We will use the expression "core-polarization" charge to describe this component of the total "effective" charge.

Microscopic calculations must be carried out in order to obtain the full momentum transfer dependence of the longitudinal effective charge as well as to obtain the analogous correction for the transverse form factor. Such a calculation must be able to successfully describe the properties of both the ground-state single-particle wave functions and the giant quadrupole resonance, and it must also describe the coupling between these two states. The key ingredient for all of these calculations is the nuclear interaction which is used. The appropriate interaction is not easy to arrive at since the free nucleon–nucleon interaction itself must be renormalized to take into account the model-space truncation. Our approach in this work is to consistently use a phenomenological interaction which has been designed to sucessfully reproduce many of the ground-state and giant-resonance-state properties of the closed-shell nuclei over a wide mass region. All aspects of our calculations are carried out using the a Skryme-type interaction. It is in this way that our work differs from previous work on the calculations of electron scattering form factors which have used finite-range two-body interactions [5,6]) and schematic two-body interactions [7,8]).

In particular, we have used the SGII Skyrme interaction [9,10]). This interaction has several advantages over previous Skyrme-type interactions. It keeps reasonable ground-state properties, while having a lower compression modulus of $K_\infty =$ 215 MeV [ref. [9])]. It also gives realistic properties for the giant resonances including the spin–isospin modes [10]). Moreover, the SGII interaction has an attractive pairing matrix element for the particle–particle-type two-body correlation. These improvements are mainly due to the introduction of a lower power of the density dependence and a modification of the spin-exchange terms for the velocity-dependent parts of the interaction.

We have studied the core-polarization effect on the single-particle electromagnetic transitions based on the self-consistent Hartree–Fock (HF) and the random-phase-approximation (RPA) theory. We first calculate the single-particle wave functions using the Skyrme-type effective interaction and the RPA response function is also obtained by using the same interaction. Core polarization is taken into account by the particle-vibration-coupling model. We will describe a summary of RPA response-function theory and the formulas for the perturbation calculation in the sect. 2. The numerical results for the single-particle transitions in the vicinity of ^{40}Ca are discussed in the sect. 3. A summary is given in the sect. 4.

2. Formulation

2.1. RPA RESPONSE-FUNCTION CALCULATION

Starting from the time-dependent Hartree–Fock theory (TDHF), we can derive the RPA Green function as a small-amplitude approximation [11]):

$$G_{\mathrm{RPA}}(\boldsymbol{r}_1, \boldsymbol{r}_2; E) = G_0(\boldsymbol{r}_1, \boldsymbol{r}_2; E) + \int G_{\mathrm{RPA}}(\boldsymbol{r}_1, \boldsymbol{r}'; E)\, V_{\mathrm{ph}}(\boldsymbol{r}')\, G_0(\boldsymbol{r}', \boldsymbol{r}_2; E)\, \mathrm{d}\boldsymbol{r}' , \quad (1)$$

where G_0 is the unperturbed ph Green function, $V_{\rm ph}$ is the residual ph interaction, and E is the excitation energy. The unperturbed response G_0 is expressed as

$$G_0(\boldsymbol{r}_1, \boldsymbol{r}_2; E) = \sum\!\!\!\!\!\!\int_{p,h} \phi_h^*(\boldsymbol{r}_1)\phi_p(\boldsymbol{r}_1) \times\{(\varepsilon_p - \varepsilon_h - E + i\eta)^{-1} + (\varepsilon_p - \varepsilon_h + E - i\eta)^{-1}\}\phi_h(\boldsymbol{r}_2)\phi_p^*(\boldsymbol{r}_2)\,, \tag{2}$$

where ε_h and ϕ_h (ε_p and ϕ_p) are the energies and wave functions of occupied (unoccupied) Hartree–Fock states calculated with $V(\boldsymbol{r}_1, \boldsymbol{r}_2)$. The symbol $\sum\!\!\!\!\!\!\int$ in eq. (2) means summation over discrete states and integration over continuous states.

The sum on particle states can be extended to all particle and hole states since every hole–hole (hh) contribution from the first term in the bracket will be cancelled by a corresponding contribution from the second term. This summation on all states can be expressed in a closed form,

$$\sum\!\!\!\!\!\!\int_{p} \phi_p(\boldsymbol{r}_1)\{(\varepsilon_p - \varepsilon_h - E + i\eta)^{-1}\}\phi_p^*(\boldsymbol{r}_2) = \langle \boldsymbol{r}_1|(H_0 - \varepsilon_h - E + i\eta)^{-1}|\boldsymbol{r}_2\rangle\,, \tag{3}$$

where H_0 is the Hartree–Fock hamiltonian. When one uses the Skyrme-type interaction, eq. (3) becomes a differential operator equation and is easy to solve numerically (it would be an integrodifferential equation for a finite-range interaction). In this way, one can avoid the problem of truncating the particle–hole (ph) configuration space. Moreover, one can take into account the single-particle continuum effect on the width of the resonance by solving the RPA Green function in the coordinate space [12,9]). We require a self-consistent treatment for the calculations of G_0 and $V_{\rm ph}$. Both quantities should be obtained from the same two-body interaction $V(\boldsymbol{r}_1, \boldsymbol{r}_2)$ in this treatment of the response function.

Once eq. (1) has been solved for a given excitation energy E, we can obtain the corresponding excitation strength for a one-body operator Q. If E is above the particle-emission threshold, the transition strength $S(E)$ is obtained by

$$S(E) = \sum_n |\langle n|Q|0\rangle|^2 \delta(E - E_n) = [1/\pi]\,\mathrm{Im}\,\{\mathrm{Tr}\,[Q^+ G_{\rm RPA}(E) Q]\}\,, \tag{4}$$

while for bound states below the threshold the excitation energies and transition strengths appear as real poles and residues in the response function $\mathrm{Tr}\,(Q^+ G_{\rm RPA} Q)$.

Since $G_{\rm RPA}$ behaves in the vicinity of resonance as [11])

$$\mathrm{Im}\,[G_{\rm RPA}(\boldsymbol{r}, \boldsymbol{r}'; E_{\rm res})] \propto \delta\rho(\boldsymbol{r})\delta\rho(\boldsymbol{r}')\,, \tag{5}$$

we can obtain the transition density $\delta\rho(\boldsymbol{r})$ of giant resonance by integrating one of the radial coordinate of $G_{\rm RPA}$ as

$$\delta\rho(\boldsymbol{r}) = \alpha \int \mathrm{Im}\,[G_{\rm RPA}(\boldsymbol{r}, \boldsymbol{r}'; E_{\rm res})]\,\mathrm{d}\boldsymbol{r}'\,, \tag{6}$$

where

$$\alpha^2 = B(\mathrm{E}\lambda)/[\pi S(E_{\rm res})]^2\,. \tag{7}$$

For an isolated resonance, $B(E\lambda)$ is the total integrated strength for the operator $Q = r^\lambda Y_{\lambda\mu}(\hat{r})$ over the resonance.

The two-body interaction $V(r_1, r_2)$ has density-independent terms and a density-dependent term,

$$V(r_1, r_2) = t_0(1 + x_0 P_\sigma)\delta(r_1 - r_2) + t_1(1 + x_1 P_\sigma)[\tfrac{1}{2}(k'^2 + k^2)]\delta(r_1 - r_2) + t_2(1 + x_2 P_\sigma)k' \cdot \delta(r_1 - r_2)k + \tfrac{1}{6}t_3(1 + x_3 P_\sigma)\rho^\alpha(R)\delta(r_1 - r_2), \quad (8)$$

where $R = \frac{1}{2}(r_1 + r_2)$, $k = (\vec{\nabla}_1 - \vec{\nabla}_2)/2i$ and $k' = (\vec{\nabla}_1 - \vec{\nabla}_2)/(-2i)$. The parameters are selected for having reasonable values for the Landau parameters in comparison with the renormalised G-matrix calculations while keeping realistic properties in the Hartree–Fock calculations [10]. We use the parameter set SGII ($t_0 = -2645$ MeV · fm^3, $t_1 = 340$ MeV · fm^5, $t_2 = -41.9$ MeV · fm^5, $t_3 = 15595$ MeV · fm^6, $x_0 = 0.09$, $x_1 = -0.0588$, $x_2 = 1.425$, $x_3 = 0.06044$, $\alpha = \frac{1}{6}$) for the following calculations since this interaction gives a successful description for various nuclear collective excitations. The residual interaction V_{ph} can be derived by taking the second derivative of the energy density for eq. (8) with respect to densities [11]. This procedure is equivalent to the Landau prescription in the Fermi liquid theory. The ph interaction is given explicitly as

$$\begin{aligned} V_{ph} &= \delta^2 E(\rho)/\delta\rho\delta\rho \\ &= \delta(r_{12})\{a + b[\nabla_1^2 + \nabla_2^2 + \nabla_{1'}^2 + \nabla_{2'}^2 \\ &\quad - (\nabla_1 - \nabla_{1'})(\nabla_2 - \nabla_{2'})] + c(\nabla_1 + \nabla_{1'})(\nabla_2 + \nabla_{2'})\} \end{aligned} \quad (9)$$

with

$$\begin{aligned} a &= \tfrac{3}{4}t_0 + \tfrac{3}{48}(\alpha + 2)(\alpha + 1)t_3\rho^\alpha \\ &\quad - \tfrac{1}{48}t_3(1 + 2x_3)\alpha(\alpha - 1)\rho_t^2\rho^\alpha/\rho^2 \\ &\quad - [\tfrac{1}{4}t_0(1 + 2x_0) + \tfrac{1}{24}t_3(1 + 2x_3)\rho^\alpha]\vec{\tau} \cdot \vec{\tau}, \\ b &= -\tfrac{1}{32}\{3t_1 + t_2(5 + 4x_2) + [t_2(1 + 2x_2) - t_1(1 + 2x_1)]\vec{\tau} \cdot \vec{\tau}\}, \\ c &= \tfrac{1}{32}\{3t_1 - 3t_2(5 + 4x_2) - [t_1(1 + 2x_1) + 3t_2(1 + 2x_2)]\vec{\tau} \cdot \vec{\tau}\}, \end{aligned} \quad (10)$$

where $\rho_t = \rho_n - \rho_p$. In eq. (9), the indices 1, 1′ refer to the ph coordinates to the left and 2, 2′ are those to the right. The spin-dependent terms are discarded in eq. (10).

2.2. FORM FOR THE OPERATORS IN THE HELICITY FORMALISM

In our calculations it is practical to use the helicity representations of the operators and the states in which most of the expectation values of the one-body operators can be written by using only the Clebsch–Gordan coefficients [13,11]. The δ-type interaction can be transformed into the helicity coordinate by the following simple

form:

$$V(\boldsymbol{r}_1, \boldsymbol{r}_2) = \delta(\boldsymbol{r}_1 - \boldsymbol{r}_2)\boldsymbol{\sigma}_1 \cdot \boldsymbol{\sigma}_2 \boldsymbol{\nabla}_1 \cdot \boldsymbol{\nabla}_2$$
$$= \sum_{\alpha,\beta,\lambda,\mu} [\delta(r_1 - r_2)/(r_1 r_2)](2\lambda+1)/(4\pi)$$
$$\times \sigma^{+}_{1\alpha} \nabla^{+}_{1\beta} D^{*\lambda}_{\mu\gamma}(\hat{\boldsymbol{r}}_1) D^{\lambda}_{\mu\gamma}(\hat{\boldsymbol{r}}_2) \sigma_{2\alpha} \nabla_{2\beta}\,, \tag{11}$$

where $\gamma = \alpha + \beta$. The electromagnetic transition operators are also rewritten as

$$T(\mathrm{C}\lambda) = \sum_i (\tfrac{1}{2} - t_{zi}) f_\lambda(r_i)\, Y_\lambda(\hat{\boldsymbol{r}}_i)$$
$$= \sum_i (\tfrac{1}{2} - t_{zi}) f_\lambda(r_i) [(2\lambda+1)/4\pi]^{1/2} D^{\lambda}_{\mu 0}(\hat{\boldsymbol{r}}_i)\,, \tag{12}$$

$$T_{\mathrm{spin}}(\mathrm{E}\lambda/\mathrm{M}\lambda) = \sum_i [\lambda(2\lambda+1)]^{1/2} f_{l\lambda}(r_i) [\tfrac{1}{2} g_s(i)] [Y_l(\hat{\boldsymbol{r}}_i) \times \sigma_i]_\lambda$$
$$= \sum_i [(2\lambda+1)/4\pi]^{1/2} f_{l\lambda}(r_i) \tfrac{1}{2} g_s(i) \{F_1(\lambda) D^{\lambda}_{\mu 0} \sigma_0 + F_2(\lambda) D^{\lambda}_{\mu 1} \sigma_{+1}\}\,, \tag{13}$$

where $\lambda = l \pm 1$ corresponds to the transverse magnetic operator, while $\lambda = l$ corresponds to the transverse electric operator. The convection current contribution to the transverse electric form factor has the same form as eq. (13) but with $\boldsymbol{\sigma}$ replaced by the operator $\vec{\nabla} - \vec{\nabla}$ and g_s replaced by g_l. Finally the orbital part of the Mλ operator for $\lambda = l \pm 1$ is given by

$$T_{\mathrm{orbit}}(\mathrm{M}\lambda) = \sum_i [2 g_l(i)/(\lambda+1)] f_{l\lambda}(r_i) [Y_l(\hat{\boldsymbol{r}}_i) \times \boldsymbol{l}_i]_\lambda$$
$$= \sum_i [(2\lambda+1)/8\pi]^{1/2} [4 g_l(i)/(\lambda+1)] f_{l\lambda}(r_i) F_3(\lambda) D^{\lambda}_{\mu 1} l_{+1}\,. \tag{14}$$

In these equations F_1, F_2 and F_3 are given by

$$F_1(\lambda = l-1) = -[\lambda(\lambda+1)]^{1/2}\,, \qquad F_2(\lambda = l-1) = (2)^{1/2}\lambda\,,$$
$$F_1(\lambda = l) = 0\,, \qquad F_2(\lambda = l) = -[2\lambda(2\lambda+1)]^{1/2}\,,$$
$$F_1(\lambda = l+1) = \lambda\,, \qquad F_2(\lambda = l+1) = [2\lambda(\lambda+1)]^{1/2}\,,$$
$$F_3(\lambda = l-1) = \lambda\,,$$
$$F_3(\lambda = l) = -[\lambda(2\lambda+1)]^{1/2}\,,$$
$$F_3(\lambda = l+1) = [\lambda(\lambda+1)]^{1/2}\,. \tag{15}$$

We propagate the operators which are included in the interaction eq. (9) in order to calculate G_{RPA}. For spin-independent excitations, we will take 6 propagators $\{1, \boldsymbol{\nabla}_1^2 + \boldsymbol{\nabla}_2^2 + \boldsymbol{\nabla}_{1'}^2 + \boldsymbol{\nabla}_{2'}^2, (\boldsymbol{\nabla}_1 \pm \boldsymbol{\nabla}_{1'})_0$ and $(\boldsymbol{\nabla}_1 \pm \boldsymbol{\nabla}_{1'})_{+1}\} \times [(2\lambda+1)/4\pi]^{1/2} D^{\lambda}_{\mu 0}$. We also have to include spin-dependent propagators $D^{\lambda}_{\mu 1}\ \sigma_{+1}$ and $D^{\lambda}_{\mu 0}\ \sigma_0$ for calculating the magnetic transition strength and the electric transverse form factor. Altogether, 8 propagators are taken into account in the response function G_{RPA}.

2.3. PERTURBATION FORMULAE FOR THE CORE POLARIZATION DUE TO RPA EXCITATIONS

We use perturbation theory to calculate the core-polarization effect due to the giant resonances. The modified single-particle wave function is expressed as

$$|\tilde{i}\rangle = |i\rangle + \sum_{j,\lambda,\omega_\lambda} \langle (j\times\omega_\lambda)i|V_{\rm ph}|i\rangle [\varepsilon_i - (\varepsilon_j + \omega_\lambda)]^{-1} |(j\times\omega_\lambda)i\rangle . \tag{16}$$

The reduced matrix element for the one-body operator is modified as [14,6])

$$\langle \tilde{j}||T_\lambda||\tilde{i}\rangle = \langle j||T_\lambda||i\rangle + \sum_{\omega_\lambda} [2\omega_\lambda/[(\varepsilon_{ij})^2 - (\omega_\lambda)^2]]\langle V_{\rm ph}\rangle \langle \omega_\lambda||T_\lambda||0\rangle/(2\lambda+1)^{1/2} , \tag{17}$$

where $\varepsilon_{ij} = \varepsilon_i - \varepsilon_j$. The major contributions to the residual interaction $V_{\rm ph}$ come from $t_0(1+x_0P_\sigma)$ and $t_3(1+x_3P_\sigma)\rho^\alpha$, and the velocity-dependent terms t_1 and t_2 have small contributions for the spin-independent matrix elements. We take into account the velocity-dependent terms in eq. (9) by using the Fermi-gas approximation. Then $V_{\rm ph}$ becomes

$$\begin{aligned} V_{\rm ph}^{\rm IS}(\boldsymbol{r}_1, \boldsymbol{r}_2) &= \{\tfrac{3}{4}t_0 + \tfrac{3}{48}(\alpha+2)(\alpha+1)t_3\rho^\alpha(R) \\ &\quad + \tfrac{1}{8}k_{\rm F}^2[3t_1 + t_2(5+4x_2)]\}\delta(\boldsymbol{r}_1 - \boldsymbol{r}_2) , \\ V_{\rm ph}^{\rm IV}(\boldsymbol{r}_1, \boldsymbol{r}_2) &= \{-\tfrac{1}{4}t_0(1+2x_0) - \tfrac{1}{24}t_3(1+2x_3)\rho^\alpha(R) \\ &\quad + \tfrac{1}{8}k_{\rm F}^2[t_2(1+2x_2) - t_1(1+2x_1)]\}\delta(\boldsymbol{r}_1 - \boldsymbol{r}_2) , \end{aligned} \tag{18}$$

where the Fermi momentum $k_{\rm F}$ is taken to be 1.33 fm^{-1}. In this approximation, the effect of the velocity-dependent terms is to renormalize the t_0 and x_0 to the effective values

$$t_0^* = -2476.5\ (\text{MeV}\cdot\text{fm}^3) , \qquad x_0^* = 0.0478 , \tag{19}$$

while the original t_0 and x_0 values of SGII interaction are $t_0 = -2645$ (MeV · fm^3) and $x_0 = 0.09$. For the simplified interaction of eq. (18) the isoscalar (β = IS) and isovector (β = IV) matrix elements $\langle V_{\rm ph}\rangle$ can be expressed in a simple form,

$$\langle V_{\rm ph}^\beta\rangle = \int r^2\,{\rm d}r\, V_{\rm ph}^\beta(r)\delta\rho_\lambda^\beta R_{\rm f}(r)R_{\rm i}(r)\langle {\rm f}|t|{\rm i}\rangle\langle {\rm f}||Y_\lambda||{\rm i}\rangle , \tag{20}$$

where $t = 1$ for IS and $t = \tau_z$ for IV. $\delta\rho_\lambda^\beta$ is the transition density of the giant resonance and $R(r)$ is the radial wave function of the single-particle state.

3. Results

We show in fig. 1 the RPA response for the isoscalar (IS) and isovector (IV) quadrupole operators $r^2Y_{2\mu}$, $r^2Y_{2\mu}\cdot\tau_z$ in ^{40}Ca. The IS collective resonance appears as a sharp peak at $E_{\rm x} = 16.7$ MeV exhausting 67% of the energy-weighted sum rule

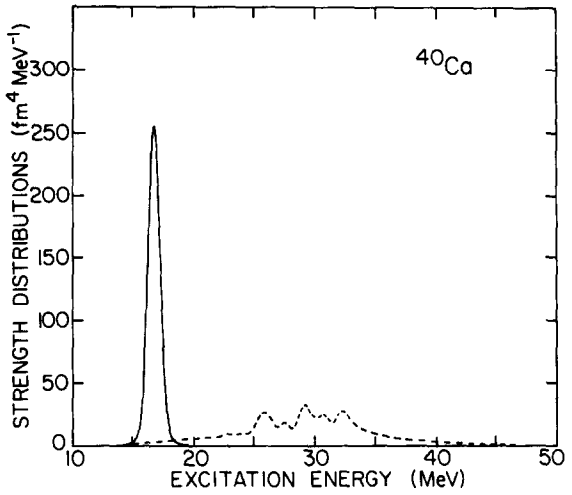

Fig. 1. The response functions for the isoscalar and isovector quadrupole transitions in ^{40}Ca. The solid and dashed curves correspond to IS and IV excitations, respectively. For the purpose of presentation the response functions are averaged over a gaussian shape with a width of 1 MeV. (The calculated decay width of the isoscalar state is about 200 keV.)

(EWSR) of 9084 MeV · fm^4, while the isovector resonance is spread out in the energy region $E_x = 25$–35 MeV. The observed IS giant resonance is concentrated in a 3 MeV wide bump around $E_x = 18$ MeV with a minor peak at $E_x = 14$ MeV which together exhaust about 70% of the EWSR value [15]). The strength function of the IV giant resonances between 25–35 MeV has about 71% of the isovector EWSR value of $9084(1+\kappa)$ MeV · fm^4, where $\kappa = 0.27$ is the enhancement factor for the SG2 interaction [16]). The rest of EWSR value lies in the high-energy region and the transition strength itself is very small. We take into account only these strong resonances in the core-polarization calculations since the high-energy tail of the strength distribution gives a relatively small contribution. The isoscalar results for ^{16}O are EWSR = 2236 MeV · fm^4 with the IS state at $E_x = 20.3$ MeV exhausting 75% of the EWSR.

The major contribution to the core polarization comes from the isoscalar resonance and we first discuss this in terms of the isoscalar effective charge. In table 1 we give the isoscalar contributions for the 1s0d single-particle matrix elements for the particle states in ^{16}O and the hole states in ^{40}Ca. The proton and neutron effective charges are based on eq. (17) with the T_λ operator taken at zero momentum transfer (i.e. with $f_\lambda(r_i) = r_i^\lambda$) and are defined as the ratios

$$\delta e_p = 1 - [\langle \tilde{j}||T_\lambda(q=0)||\tilde{i}\rangle_\pi / \langle j||T_\lambda(q=0)||i\rangle_\pi],$$

$$\delta e_n = \langle \tilde{j}||T_\lambda(q=0)||\tilde{i}\rangle_\nu / \langle j||T_\lambda(q=0)||i\rangle_\pi .$$

We can separate the contributions from the isoscalar and isovector resonances to these effective charges and express them in the form $\delta e_p = \delta e_p^{IS} - \delta e_p^{IV}$ and $\delta e_n =$

TABLE 1

Isoscalar contribution δe^{IS} to the proton and neutron core-polarization charges for the 1s0d particle states in ^{16}O and hole states in ^{40}Ca

f	i	^{16}O		^{40}Ca	
		π	ν	π	ν
$0d_{3/2}$	$0d_{3/2}$	0.155	0.176	0.406	0.396
$0d_{3/2}$	$0d_{5/2}$	0.269	0.288	0.473	0.465
$1s_{1/2}$	$0d_{3/2}$	0.151	0.168	0.450	0.436
$0d_{5/2}$	$0d_{5/2}$	0.359	0.361	0.423	0.413
$1s_{1/2}$	$0d_{5/2}$	0.251	0.265	0.495	0.489

$\delta e_n^{IS} + \delta e_n^{IV}$. Except for some relatively small differences due to the difference between the proton and neutron radial wave functions, $\delta e_p^{IS/IV}$ is nearly equal to $\delta e_n^{IS/IV}$. The "isoscalar" and "isovector" effective charges will be defined by $\delta e^{IS} = \frac{1}{2}(\delta e_n + \delta e_p)$ and $\delta e^{IV} = \frac{1}{2}(\delta e_n - \delta e_p)$.

We first discuss the state dependence of the results for δe^{IS}. For the degenerate oscillator states it is worthwhile to remember that with a central interaction connecting the particle and vibration that the effective charge is independent of the initial and final total angular momenta $j_f - j_i$ for a given combination of the orbital angular momenta $l_f - l_i$ and for a given core [17]). We use a central force but there is still some orbital dependence in our results due to the difference between the HF and oscillator radial wave functions and to the splitting of the single-particle state via ε_{ij} in eq. (17). The effect of ε_{ij} is to increase the effective charge for the off-diagonal matrix elements relative to the diagonal matrix elements. The effect of the HF radial wave functions is primarily to reduce the value of the core-polarization charge when the nucleons are loosely bound and have a large mean-square radius.

In ref. [18]) it was argued that the radial wave function dependence of the effective charge is empirically roughly proportional to some power of the ratio G which is defined as the matrix element of r^2 calculated with the HF single-particle radial wave functions divided by this matrix element calculated with harmonic-oscillator radial wave functions:

$$G = \langle \mathrm{f}|r^2|\mathrm{i}\rangle_{\mathrm{HF}} / \langle \mathrm{f}|r^2|\mathrm{i}\rangle_{\mathrm{HO}} . \tag{21}$$

These ratios for our calculation are given in table 2. The power depends on the range of the interation which connects the single-particle state and vibration and varies empirically from about -2 for a zero-range delta interaction to 0 (i.e. the effective charge is independent of the radial wave function) for the long-range $Q \cdot Q$ interaction. If we do not include the density dependence in eq. (18) (and thus just have a delta interaction) this power in our case is about -1.6 and with the full density-dependent interaction the power is closer to about -1.3. Thus the effect of

TABLE 2

The values of G defined by eq. (21) for the configurations involved in the 1s0d shell E2 transitions

f	i	^{16}O		^{40}Ca	
		π	ν	π	ν
$0d_{3/2}$	$0d_{3/2}$	1.936	1.524	1.002	0.965
$0d_{3/2}$	$0d_{5/2}$	1.198	1.114	0.979	0.948
$1s_{1/2}$	$0d_{3/2}$	1.882	1.535	0.991	0.949
$0d_{5/2}$	$0d_{5/2}$	1.027	0.981	0.962	0.935
$1s_{1/2}$	$0d_{5/2}$	1.183	1.091	0.950	0.918

For the harmonic-oscillator radial wave functions values of $b = 1.769$ fm for ^{16}O and $b = 1.963$ fm for ^{40}Ca were used.

the density dependence is to slightly reduce the state dependence of the effective charge.

The empirical isoscalar effective charge in the mass region $A = 20$–36 has been obtained from a comparison of the experimental E2 matrix elements with those calculated with the full multi-particle $(0d1s)^n$ wave functions [18,1]). Over this mass region the empirical isoscalar effective charge is remarkably state and mass independent with an average value of 0.35 ± 0.05. To compare this with the results given in table 1 we should take into account that the multi-particle matrix elements are dominated by the $0d_{5/2}$-$0d_{5/2}$ ($\delta e_{\rm th} = 0.36$) and $0d_{5/2}$-$1s_{1/2}$ ($\delta e_{\rm th} = 0.25$) terms at the beginning of the shell and by the $0d_{3/2}$-$0d_{3/2}$ ($\delta e_{\rm th} = 0.40$) term at the end of the shell. The average of the theoretical results given above in brackets is 0.34 in excellent agreement with the empirical value of 0.35 ± 0.05. It will be interesting in the future to try to extract from the multi-particle data the orbit dependence suggested by the present calculations.

Zamick *et al.* pointed out that a short-range interaction gives a very large core-polarization charge, $\delta e^{\rm IS} = 0.85$, for the quadrupole transition in the case of ^{40}Ca [ref. [19])]. We have also done a schematic calculation using only $t_0(1 + x_0 P_\sigma)$ and $t_3(1 + x_3 P_\sigma)\rho^\alpha$ interactions with the parameters $t_0 = -1094$ MeV $\cdot$ fm^3, $x_0 = 0.609$, $t_3 = 19750$ MeV $\cdot$ fm^6, $x_3 = 1$ and $\alpha = 1$. This parameter set gives a resonable mean charge radius and binding energy for ^{40}Ca. However, the energy of IS giant resonance comes down from $E_x = 16.7$ MeV to $E_x = 13.0$ MeV and the transition strength is increased from $B(E2) = 388e^2 \cdot \text{fm}^4$ to $B(E2) = 563e^2 \cdot \text{fm}^4$. These changes give the core-polarization charge $\delta e^{\rm IS} = 1.1$ for the $(0d_{3/2} \rightarrow 1s_{1/2})_\pi$ transition instead of $\delta e^{\rm IS} = 0.45$ coming from the full interaction. The velocity-dependent terms $t_1(1 + x_1 P_\sigma)$ and $t_2(1 + x_2 P_\sigma)$ are crucial to obtain a reasonable energy for the isoscalar giant quadrupole resonance and hence also for the amount of core-polarization charge.

The effect of the velocity-dependent terms can be qualitatively related to the role of the effective mass m^*/m in the excitation energy of the giant resonance. In the

harmonic-oscillator approximation the single-particle energy spacing and the resonance excitation energy are proportional to $(m^*/m)^{-1/2}$ [ref. [13]), p. 511 and ref. [20])]. The velocity-dependent SGII interaction has a nuclear-matter effective mass of $m^*/m = 0.79$ and the velocity-independent interaction has $m^*/m = 1$. Going from $m^*/m = 0.79$ to $m^*/m = 1$, lowers the excitation energy by about 11% in the oscillator approximation, which can be compared to the lowering of 22% in our Hartree–Fock RPA calculation.

Next we discuss the isovector contribution to the single-hole matrix elements in ^{40}Ca. The results are given in table 3 for the average contribution to the proton and neutron. As can be noted for the ^{40}Ca isoscalar case in table 1, the difference of the individual proton and neutron values from the average is relatively small. The factor of 4 difference between the IS and IV core-polarization charges is due to several effects. The energy dependence ω_λ in eq. (17) induces a factor 2 difference between δe^{IS} to δe^{IV} since $\omega^{IS} = 16.7$ MeV while ω^{IV} is around 30 MeV. Also the $B(E2)$ value comes out to be a factor 1.6 different, i.e. $B(E2) = 388e^2 \cdot \text{fm}^4$ for IS case and $B(E2) = 246e^2 \cdot \text{fm}^4$ for IV resonances between $E_x = 25$–35 MeV. The transition matrices which appear twice in the last term of eq. (17), i.e. in $\langle V \rangle$ and $\langle \omega_\lambda || T_\lambda || 0 \rangle$, thus give an additional factor of 1.6. Finally there is a factor of about 1.3 difference between the strength of the IS and IV ph interactions.

The empirical isovector effective charge for the sd-shell nuclei has proved difficult to obtain because it is sensitive to what is assumed for the valence radial wave functions [18]). The empirical results range from a value of $e_p - e_n = 1.0$ (the free nucleon value) obtained with a harmonic oscillator potential to a smaller value of $e_p - e_n = 0.35$ obtained with a non-local (energy-dependent) Woods–Saxon potential. An intermediate value of $e_p - e_n = 0.67$ was obtained with the local (energy-independent) Woods-Saxon potential [18]). Thus for $\delta e^{IV} = \frac{1}{2}(e_n - e_p + 1)$ we have a wide range of empirical values from 0 to +0.16 to +0.32. The present result of +0.11 fits in this range and agrees best with the local Woods-Saxon analysis of ref [18]).

TABLE 3

Isoscalar (IS) and isovector (IV) contributions to the core-polarization charges for the 1s0d hole states in ^{40}Ca

f	i	IS	IV	π	ν
$0d_{3/2}$	$0d_{3/2}$	0.401	0.110	0.291	0.511
$0d_{3/2}$	$0d_{5/2}$	0.469	0.119	0.350	0.588
$1s_{1/2}$	$0d_{3/2}$	0.443	0.101	0.342	0.544
$0d_{5/2}$	$0d_{5/2}$	0.418	0.117	0.301	0.535
$1s_{1/2}$	$0d_{5/2}$	0.492	0.108	0.384	0.600

The individual IS and IV results for protons and neutrons only differ by a few percent and hence only the average is given here. The proton and neutron core-polarization charges given are the total of the IS and IV contributions.

A more complete test of our calculations would come from a comparison with experimental electron-scattering form-factor data for the single-particle transitions $A=17$ and $A=39$. Of course, only ^{17}O and ^{39}K targets exist and for these only the $d_{5/2}$ and $s_{1/2}$ states in ^{17}O and the $d_{3/2}$ and $s_{1/2}$ states in ^{39}K exist in nature in a relatively pure form, the higher states having fragmented single-particle strength due to the mixing with core-excited states. The longitudinal C2 form factors for the elastic transitions are difficult to observe because of the dominant C0 contributions (transverse E2 for the elastic vanishes due to parity conservation). This leaves us with only two inelastic transitions to provide information on the C2 and E2 form factors. Some low-q data for ^{39}K have existed for some years [21]) and very recently at NIKHEF medium-q and high-q data have been obtained [22]). In this work we will compare our calculations with these data. Additional comparisons to some of the multi-particle sd-shell data [1]) will be part of a future work.

The form factors were calculated starting from the operators for point protons given in subsect. 2.2. The center-of-mass correction was taken into account in the usual harmonic-oscillator approximation [23]). The nucleon finite-size corrections were incorporated in the dipole approximation [ref. [13]), p. 386]. The calculations were carried out in the plane-wave Born approximation (PWBA). For this small Z-value, the PWBA C2 form factor is very close to a DWBA calculation when one takes into account the distortion effect with an effective momentum transfer value q_{eff}, except in the minima and in the rise just after the minima where the DWBA is filled in relative to PWBA [ref. [1])]. We compare our PWBA calculation plotted versus q to the experimental data plotted versus q_{eff}.

The Coulomb form factor of the quadrupole transition $(0d_{3/2}^{-1} \rightarrow 1s_{1/2}^{-1})_{\pi}$ in ^{39}K is shown in fig. 2. The dashed line corresponds to the result without core polarization, while the solid curve shows the result with core polarization. The calculated transition strength $B(\text{E2})_{\text{theory}} = 21.1 e^2 \cdot \text{fm}^4$ agrees well with the experimental one $B(\text{E2})_{\text{exp}} = 18.9 \pm 1.8 e^2 \cdot \text{fm}^4$ which is obtained at the limit $q=0$ [ref. [21])]. The q-dependence of the form factor is nicely reproduced by the calculation with core polarization. The calculation also shows quantitative agreement of the absolute magnitudes of the first peak at $q=0.75\ \text{fm}^{-1}$ and the second peak at $q=1.7\ \text{fm}^{-1}$. One of the aspects of our calculation which is important in obtaining this good agreement is the fact that the calculated HF mean square charge radius of 3.48 fm for ^{40}Ca is in agreement with the experimental value of 3.481 ± 0.005 fm [ref. [24])].

We show in fig. 3 the transition densities of IS and IV giant resonances together with that of the Tassie model,

$$\delta\rho^{\lambda}(r) \propto r^{\lambda-1} \mathrm{d}\rho_0(r)/\mathrm{d}r, \tag{22}$$

where ρ_0 is the ground-state proton density. The IS transition density is very close to the Tassie-type one, while the IV transition density of the resonance at $E_x = 29$ MeV changes sign at around $r=2$ fm. The other IV resonances have almost the same radial dependences for the transition densities as the state at $E_x = 29$ MeV. Due to

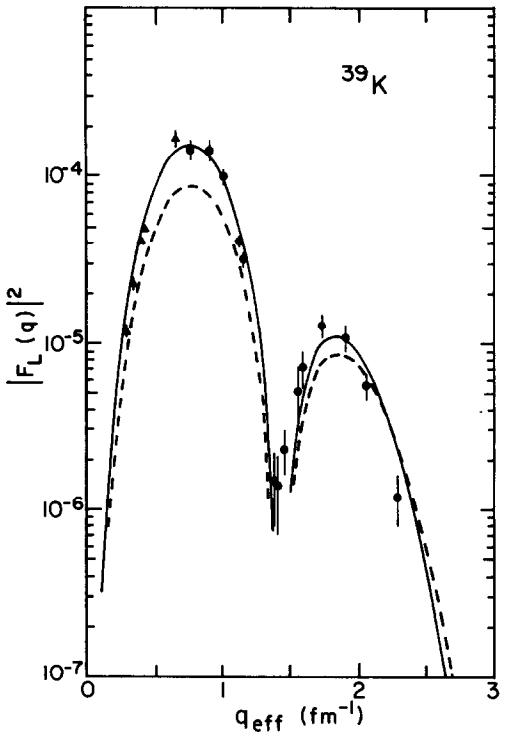

Fig. 2. The Coulomb form factor of the quadrupole transition $(0d_{3/2}^{-1} \rightarrow 1s_{1/2}^{-1})_\pi$ in ^{39}K calculated using the HF single-particle wave functions. The solid and dashed curves correspond to the HF transition density with and without core-polarization effects, respectively. The experimental data are taken from ref. [21]) (triangles) and ref. [22]) (circles).

the couplings to these resonances, the transition density for the $(0d_{3/2}^{-1} \rightarrow 1s_{1/2}^{-1})_\pi$ transition is increased at the surface region and decreased slightly in the inside of the nucleus (see fig. 4). This change of the transition density is responsible for the larger enhancement at the first peak than the second peak in the form factor in fig. 2.

The M1 and E2 transverse form factors for the $(0d_{3/2}^{-1} \rightarrow 1s_{1/2}^{-1})_\pi$ transition are shown in fig. 5. In the small-q region, the M1 and E2 form factors have almost same order of magnitude, while the E2 form factor becomes dominant in the high-q region around 2 fm^{-1}. The core-polarization effect on the E2 form factor quenches the first peak at $q = 0.9$ fm^{-1} and does not change much in the second peak. The calculated form factor follows the main features of the experimental one in the high-q region. On the other hand, in the low-q region, the theory is higher than experiment.

We have not calculated core-polarization corrections to the M1 form factor since they cannot be carried out as a straightforward generalization of the E2 calculation. Moreover, it is clear for $q = 0$ that delta-isobar admixtures, higher-order nuclear

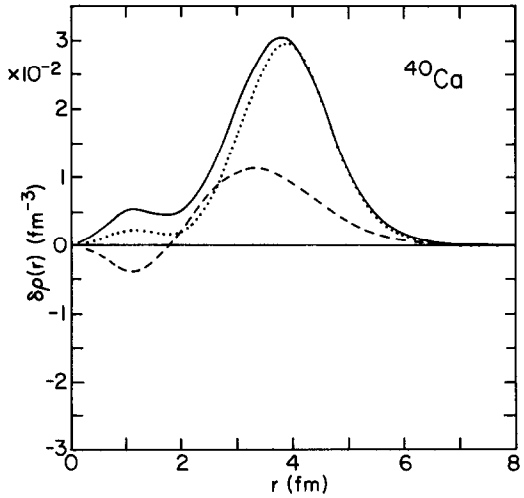

Fig. 3. The proton transition densities of giant resonances. The solid curve shows that of IS resonance at $E_x = 16.7$ MeV, while the dashed curve corresponds to the IV resonance at $E_x = 29$ MeV. The magnitude of the transition density is determined by eqs. (6) and (7) with the energy intervals $E_x = 16.2$–17.2 MeV for IS and $E_x = 28.0$–30.0 MeV for IV. The dotted curve is the transition density of the Tassie model eq. (22) with an arbitrary scale.

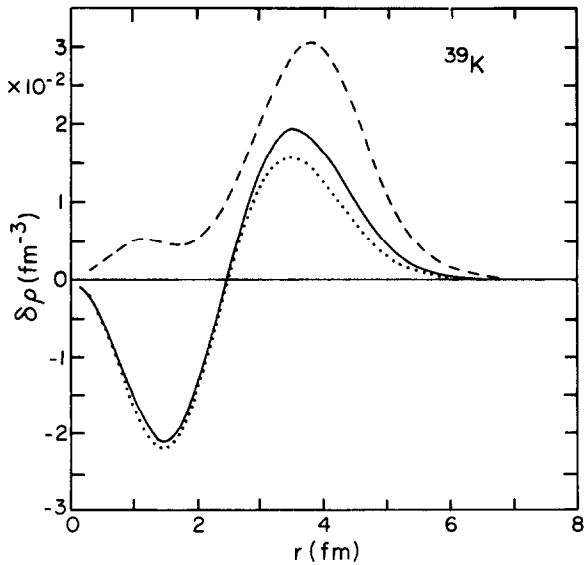

Fig. 4. The transition densities $\delta\rho^{\lambda=2}$ for the $(0d_{3/2}^{-1} \rightarrow 1s_{1/2}^{-1})_\pi$ excitation at $E_x = 2.53$ MeV in ^{39}K. The solid and dashed curves correspond to with and without core polarization, respectively. For comparison we also show the transition density for the IS resonance from fig. 3 (the dashed curve in this figure).

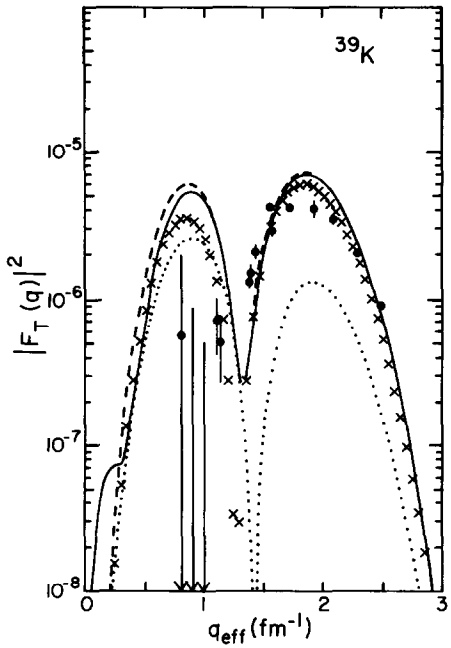

Fig. 5. The transverse form factor of the transition $(0d_{3/2}^{-1} \rightarrow 1s_{1/2}^{-1})_{\pi}$. The dotted curve corresponds to the M1 form factor, and the ×'s corresponds to the E2 form factor without core polarization. The sum of M1 and E2 form factors is shown by the solid curve (with core polarization) and the dashed curve (without core polarization). The experimental data are taken from ref. [22]).

configuration mixing and meson-exchange currents are all important for the M1 matrix element [25]) and these effects together with the first-order core polarization should be considered for a complete calculation of the transverse form factor. We should also mention that the tensor force is important for the higher-order nuclear configuration mixing [25]) and is probably also important for the first-order core-polarization and this tensor component should be added to our Skyrme interaction in order to obtain a reliable result for the transverse form factor.

4. Summary

We have studied the core-polarization effect on the electromagnetic transitions in the vicinity of ^{16}O and ^{40}Ca. The self-consistent HF+RPA method was used for calculations of the single-particle wave functions and the response functions of isoscalar and isovector giant resonances taking the Skyrme-type interaction SGII. The core-polarization effect was studied by the particle–vibration-coupling model using the same Skyrme-type interaction for the coupling hamiltonian. For the important matrix elements involved in the multi-particle sd-shell transitions we obtained an average isoscalar effective charge of $\delta e^{IS} = 0.34$ in good agreement with

the empirical result of 0.35 ± 0.05 [refs. [18,1])]. The calculated isovector effective charge is $\delta e^{IV} = 0.11$ which is consistent with the analysis of ref. [18]). For the well-bound states in ^{40}Ca the state dependence of the core-polarization charge is small and at most 20%.

We show in fig. 2 the Coulomb form factor of the transition $(0d_{3/2}^{-1} \rightarrow 1s_{1/2}^{-1})_\pi$ in ^{39}K. The calculated form factor shows good agreement with the experimental one both in the q-dependence and the absolute magnitudes of the first peak and the second peak. The core-polarization effect on the transverse form factor is shown in fig. 5. The comparison with experiment is not as good in this case and indicates the need to include delta isobars, higher-qrder nuclear configuration mixing and mesonic exchange corrections in the calculation.

We would like to thank C.W. de Jager for providing us with their ^{39}K electron scattering data before publication. This research was supported in part by the National Science Foundation grant no. PHY-83-12245.

References

1) B.A. Brown, R. Radhi and B.H. Wildenthal, Phys. Reports **101** (1983) 313
2) T. Iwamoto, H. Horie and A. Yokoyama, Phys. Rev. **C25** (1982) 658
3) J. Heisenberg, J. Dawson, T. Milliman, O. Schwentker, J. Lichtenstadt, C.N. Papanicolas, J. Wise, J.S. McCarthy, N. Hintz and H.P. Blok, Phys. Rev. **C29** (1984) 97
4) A. Bohr and B.R. Mottelson, Nuclear structure, vol. II (Benjamin, Reading, Mass., 1979)
5) Y. Horikawa, T. Hoshino and A. Arima, Nucl. Phys. **A278** (1977) 297
6) F. Petrovich, H. McManus, J. Borysowicz and G.R. Hammerstein, Phys. Rev. **C16** (1977) 839
7) I. Hamamoto, Phys. Reports **10C** (1974) 1
8) T. Suzuki, Nucl. Phys. **A217** (1973) 182; **A220** (1974) 569
9) Nguyen van Giai and H. Sagawa, Nucl. Phys. **A371** (1981) 1
10) Nguyen van Giai and H. Sagawa, Phys. Lett. **106B** (1981) 379
11) G.F. Bertsch and S.F. Tsai, Phys. Reports **18** (1975) 125
12) S. Sholomo and G.F. Bertsch, Nucl. Phys. **A243** (1975) 307
13) A. Bohr and B.R. Mottelson, Nuclear structure, vol. I (Benjamin, Reading, Mass., 1975)
14) H. Sagawa, Phys. Rev. **C19** (1979) 506
15) J. Speth and A. van der Woude, Rep. Prog. Phys. **44** (1981) 719, and references therein
16) H. Krivine, J. Treiner and O. Bohigas, Nucl. Phys. **A336** (1980) 155
17) B.A. Brown, A. Arima and J.B. McGrory, Nucl. Phys. **A277** (1977) 77
18) B.A. Brown, B.H. Wildenthal, W. Chung, S.E. Massen, M. Benas, A.M. Bernstein, R. Miskimen, V.R. Brown and V.A. Madsen, Phys. Rev. **C26** (1982) 2247
19) L. Zamick, M. Golin and S. Moszkowski, Phys. Lett. **66B** (1977) 116
20) M. Golin and L. Zamick, Nucl. Phys. **A249** (1975) 320
21) Th. Grundy, A. Richter, G. Schrieder, E. Spamer and W. Stock, Nucl. Phys. **A357** (1981) 269
22) C.W. de Jager, P.H.M. Keizer, S.W. Kowalski, L. Lapikas, E.A.J.M. Offermann and H. de Vries, Proc. Int. Conf. on nuclear physics, vol. 1, Contributed papers, Florence, 1983; and private communication
23) L.J. Tassie and F.C. Barker, Phys. Rev. **111** (1958) 940
24) H.D. Wohlfahrt, E.B. Shera, M.V. Hoehn, Y. Yamazaki and R.M. Steffen, Phys. Rev. **C23** (1981) 533
25) I.S. Towner and F.C. Khanna, Nucl. Phys. **A399** (1983) 334